Subtle Stereochemical Effects Influence Binding and Purification Abilities of an FeII4L4 Cage

Original
Subtle Stereochemical Effects Influence Binding and Purification Abilities of an FeII4L4 Cage / Xue, Weichao; Pesce, Luca; Bellamkonda, Adinarayana; Ronson, Tanya K.; Wu, Kai; Zhang, Dawei; Vanthuyne, Nicolas; Brotin, Thierry; Martinez, Alexandre; Pavan, Giovanni M.; Nitschke, Jonathan R.. - In: JOURNAL OF THE AMERICAN CHEMICAL SOCIETY. - ISSN 1520-5126. - 145:9(2023), pp. 5570-5577. [10.1021/jacs.3c00294]

Publisher:
American Chemical Society

Published
DOI:10.1021/jacs.3c00294

JACS
JOURNAL OF THE AMERICAN CHEMICAL SOCIETY

pubs.acs.org/JACS
Article

Subtle Stereochemical Effects Influence Binding and Purification Abilities of an $Fe^{II}_4L_4$ Cage

Weichao Xue, Luca Pesce, Adinarayana Bellamkonda, Tanya K. Ronson, Kai Wu, Dawei Zhang, Nicolas Vanthuyne, Thierry Brotin, Alexandre Martinez, Giovanni M. Pavan,* and Jonathan R. Nitschke*

Cite This: *J. Am. Chem. Soc.* 2023, 145, 5570−5577

Read Online

ACCESS | Metrics & More | Article Recommendations | Supporting Information

ABSTRACT: A tetrahedral $Fe^{II}_4L_4$ cage assembled from the coordination of triangular chiral, face-capping ligands to iron(II). This cage exists as two diastereomers in solution, which differ in the stereochemistry of their metal vertices, but share the same point chirality of the ligand. The equilibrium between these cage diastereomers was subtly perturbed by guest binding. This perturbation from equilibrium correlated with the size and shape fit of the guest within the host; insight as to the interplay between stereochemistry and fit was provided by atomistic well-tempered metadynamics simulations. The understanding thus gained as to the stereochemical impact on guest binding enabled the design of a straightforward process for the resolution of the enantiomers of a racemic guest.

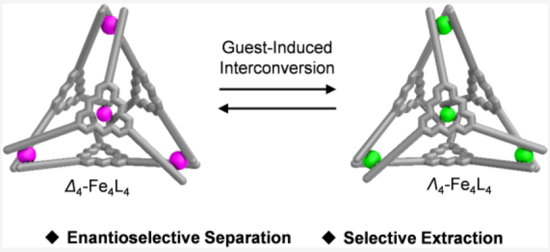

■ INTRODUCTION

Enzymes possess chirotopic cavities, enabling stereoselective recognition of target substrates and stereospecific chemical reactions.[1−3] Enantiopure metal−organic cages with enclosed cavities,[4] constructed by coordination-driven self-assembly, are able to mimic the functions of enzymes and have found uses across diverse areas, including stereoselective sensing, separation,[5] and catalysis.[6,7] Studies on the communication of stereochemistry within cages also help to elucidate the flow of stereochemical information in both artificial and living systems and may lead to the discovery of bioinspired applications.[8]

The stereochemistry of metal−organic cages can be influenced by enantiopure counterions and guests, through templation during cage formation or postassembly resolution of racemic cage mixtures.[4,9] More frequently, enantiopure components, i.e., ligands and metal complexes, are used to control the stereochemistry of self-assembled structures, whereby the resulting metal−organic cages are enantiopure.[4,10] In cases where the metal ions, particularly those from the d-block or f-block, have octahedral[11] or pseudotricapped trigonal prismatic geometry,[12] stereochemical information from the ligands can transfer to the metal vertices to produce either a preferred Δ or Λ handedness during higher-order self-assembly. Based upon this strategy, examples of the diastereoselective formation of homochiral cages, with precise control of the handedness of both metal vertices and the final assembled structure, have been reported.[4,11,12]

Metal−organic cages with electron-deficient walls have displayed extensive host−guest properties, binding electron-rich and even electron-poor guests with high affinities.[13] We therefore envisioned that the incorporation of an electron-poor ligand into a chiral cage framework might optimize binding ability,[14] resulting in the discovery of self-assembled cages with new potential applications.[15] Herein, we describe the self-assembly of an electron-deficient enantiopure ligand with Fe^{II} to afford an $Fe^{II}_4L_4$ tetrahedron existing as a pair of distinct diastereomers, adopting either an all Δ or Λ configuration of metal centers, with moderate diastereocontrol. The ratio of the Δ_4 to Λ_4 configurations was then subtly modulated and even inverted by the encapsulation of guests. The diastereoenriched cage enabled the selective encapsulation of functionalized fullerenes from mixtures and enantioselective separation of racemic cryptophane-A (CRY-A).

■ RESULTS AND DISCUSSION

Tritopic ligand **A** with pyridyl-triazole "click" chelates[14,16] was synthesized from iodinated *N*-heterotriangulene over three steps (Figure S1). The carbonyl groups and perfluorophenyl rings ensure its electron-deficient nature. The self-assembly of **A** (4 equiv) with iron(II) bis(trifluoromethanesulfonyl)imide ($Fe(NTf_2)_2$, 4 equiv) in acetonitrile at 343 K gave rise to cage **1** (Figure 1a). Its $Fe^{II}_4L_4$ composition, as anticipated following the foundational work of Lusby,[16] was confirmed by electrospray ionization mass spectrometry (ESI-MS, Figure S21). One set of proton signals in the ^1H NMR spectrum of **1**

Received: January 9, 2023
Published: February 27, 2023

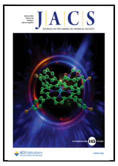

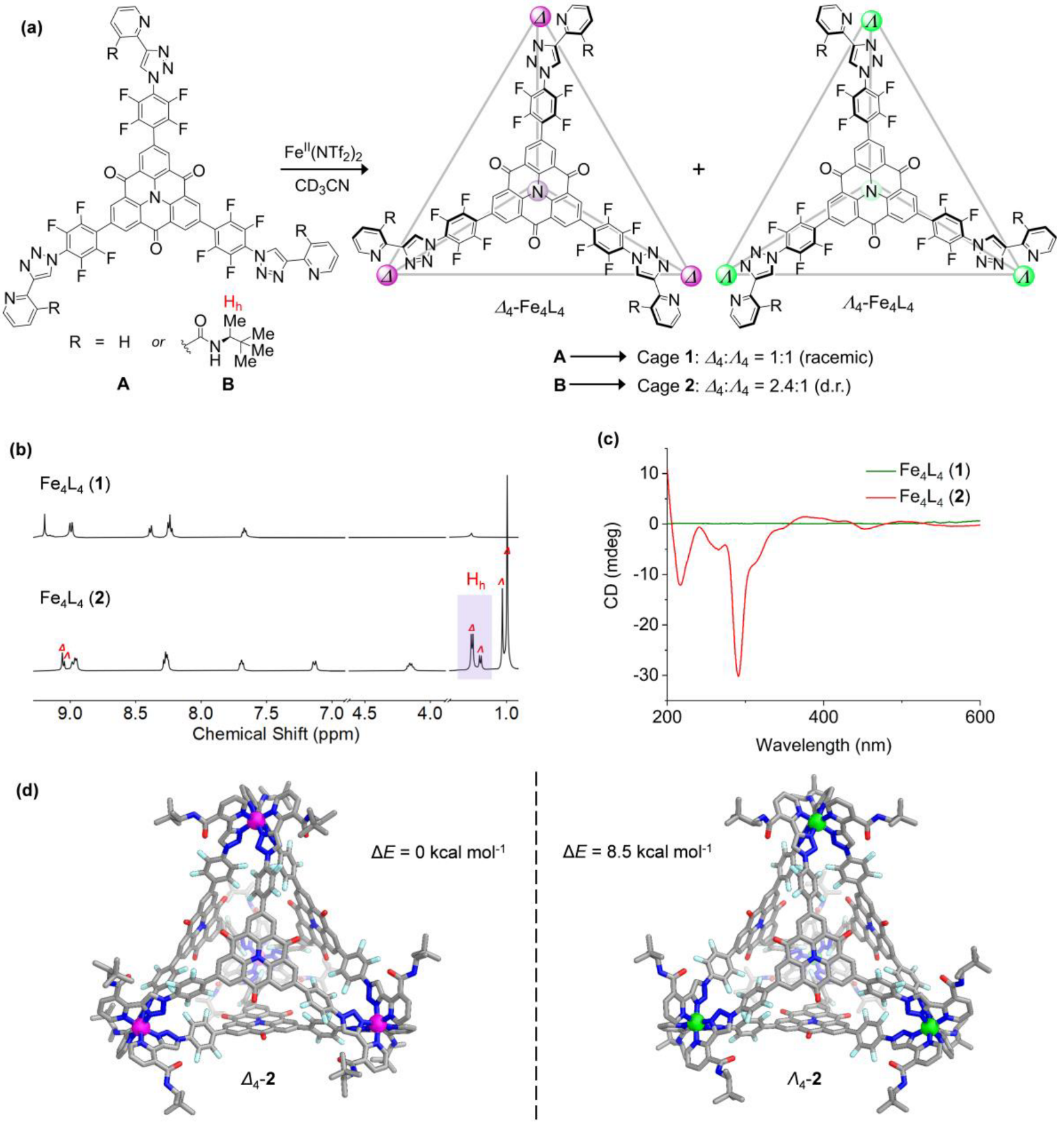

Figure 1. (a) Self-assembly of cages **1** and **2** from ligands **A** and **B**, respectively. (b) Partial ^{1}H NMR spectra of cages **1** and **2**, with H_h used to gauge the d.r. of **2** (500 MHz, CD_3CN, 298 K). (c) CD spectra of cages **1** and **2**. (d) Front view of the DFT-optimized molecular models of Δ_4-**2** and Λ_4-**2**, with ΔE representing the difference in total energy between the two diastereomers at 298 K as estimated by molecular dynamics.

indicated the exclusive formation of a *T*-symmetric framework, with each octahedral tris-chelate metal vertex displaying the same handedness (Figure 1b). The absence of Cotton effects in the circular dichroism (CD) spectrum was consistent with the formation of a racemic mixture of Δ_4-**1** and Λ_4-**1** in solution (Figure 1c).

We hypothesized that the stereochemistry of such $Fe^{II}_4L_4$ cages might be controlled by using an enantiopure ligand, which could dictate the configuration of the iron centers. Chiral ligand **B**, having the same ligand core as **A**, was therefore prepared, with each arm bearing an amide-containing chiral directing group (Figure S7). The stereocenter-containing side chain was incorporated at the 3-position of the pyridyl ring to secure its proximity to the metal vertex. Such a design should also avoid steric clash within the coordination environment around the metal centers that would be induced by substituents at the pyridyl 6-position, which might destabilize assembled structures.[17]

Ligand **B** underwent self-assembly with $Fe(NTf_2)_2$ to produce $Fe^{II}_4L_4$ cage **2** (Figure 1a), as confirmed by ESI-MS (Figure S30). The ^{1}H NMR spectrum of cage **2** shows two sets of proton signals, consistent with the formation of Δ_4-**2** and Λ_4-**2** as diastereomeric complexes. The well-separated signals of H_h allowed determination of a diastereomeric ratio (d.r.) of 2.4:1 (Figure 1b). The same diffusion coefficient was observed for all peaks in the diffusion-ordered spectroscopy (DOSY) spectrum, indicating similar hydrodynamic radii for both diastereomers (Figure S25). Other *N*-heterotriangulene-based chiral ligands bearing modified chiral directing groups were also employed in the self-assembly process; however, lower diastereomeric ratios were observed in all cases compared to the present ratio of 2.4:1 (Figures S34 and S35).

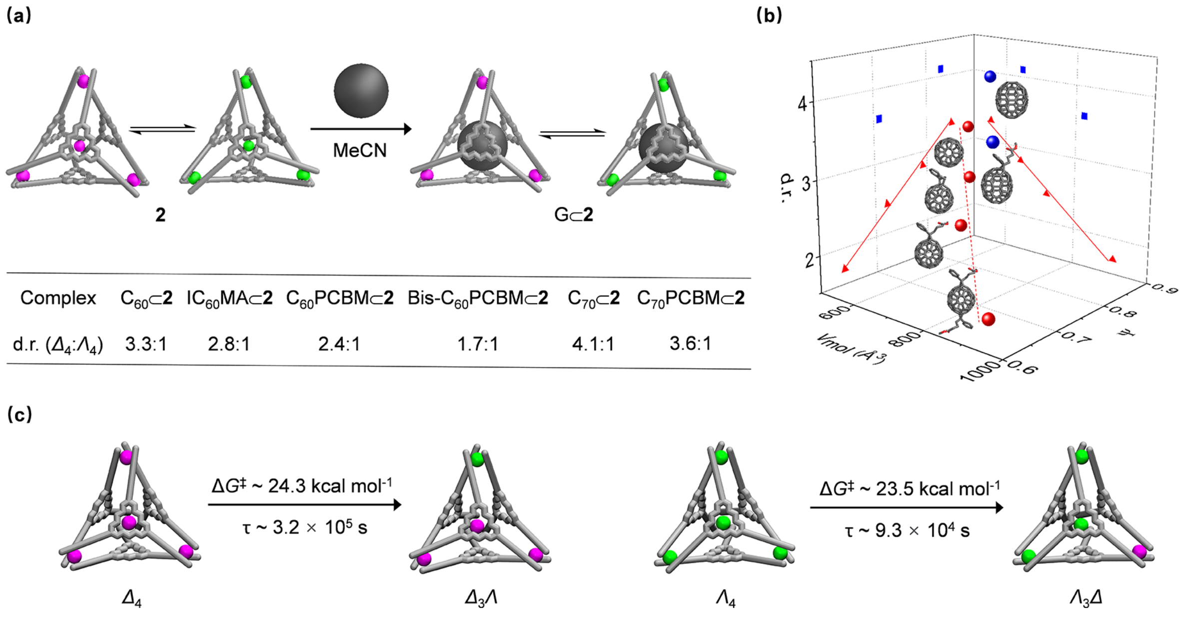

Complex	$C_{60}\subset 2$	$IC_{60}MA\subset 2$	$C_{60}PCBM\subset 2$	Bis-$C_{60}PCBM\subset 2$	$C_{70}\subset 2$	$C_{70}PCBM\subset 2$
d.r. (Δ_4:Λ_4)	3.3:1	2.8:1	2.4:1	1.7:1	4.1:1	3.6:1

Figure 2. (a) Schematic and table showing guest-binding-induced $\Delta_4 \rightleftarrows \Lambda_4$ interconversion, with d.r. determined by ^{1}H NMR. (b) Diastereomeric ratio of the host−guest complex plotted against the molecular volume (V_{mol}) and sphericity (Ψ) of guests. PCBM = [6,6]-phenyl-C_n-butyric acid methyl ester (n = 61 or 71). $IC_{60}MA$ = indene-C_{60} monoadduct. Bis-C_{60}PCBM exists as a mixture of regioisomers. C_{70}PCBM exists as a mixture of regioisomers with about 85% α-C_{70}PCBM. (c) Schematic showing conversion of one metal vertex within the framework of **2**, with $\Delta G^‡$ representing the calculated transition energy barrier and τ representing the characteristic transition timescale at 298 K.

The CD spectrum of cage **2** displayed intense negative signals around 240−340 nm, corresponding to high-energy π−π* transitions in the ligands, while metal-to-ligand charge transfer (MLCT) and d−d transitions produced weaker signals from 360 to 540 nm (Figure 1c). The Cotton effects observed in the CD spectrum are correlated with the handedness of the octahedral tris-chelate iron vertices. Comparison of the CD spectra of structurally similar Δ- and Λ-$[Fe(bpy)_3]^{2+}$ complexes, particularly peaks resulting from π−π* and MLCT transitions, allowed us to infer there is an excess of iron centers having Δ configuration within cage **2**.[18,19] The major diastereomer of **2** was thus determined to be Δ_4-**2**, and the minor diastereomer was Λ_4-**2**.

After many unsuccessful attempts to grow crystals suitable for X-ray diffraction, we undertook density functional theory (DFT) calculations to obtain the energy-minimized molecular models of Δ_4-**2** and Λ_4-**2** (Figure 1d; for details, see Supporting Information Section 10).[20] In accordance with previous observations of face-capped M_4L_4 tetrahedral cages,[5i,9h] Δ_4-**2** adopts a clockwise orientation of its four ligand faces, while Λ_4-**2** is paired with ligands of anticlockwise orientation. The $Fe^{II}\cdots Fe^{II}$ distances in both diastereomers are similar (ca. 23 Å). The calculated cavity volumes are only slightly different: 1281 Å^3 for Δ_4-**2** and 1266 Å^3 for Λ_4-**2** (Figure S107).[21]

In control experiments, an $Fe^{II}L_3$ complex was formed by the reaction of $Fe(NTf_2)_2$ with a monomeric pyridyl-triazole ligand bearing the same chiral side chain (Figure S36). Very weak signals observed in the CD spectrum indicated a weaker chiral induction effect in this mononuclear complex relative to that of the tetranuclear cage (Figure S38). These results reflect that diastereoselectivity during the formation of **2** emerges as a result of higher-order assembly, in which the stereochemical information transfer from ligand to metal vertex and stereochemical communication between metal centers may cooperatively play a role in amplifying the energy differences between the two diastereomers.[22]

The relative energy differences (ΔE) between Δ_4-**2** and Λ_4-**2** was gauged to be 8.5 kcal mol^{-1} by performing molecular dynamics simulations on a model of cage **2** in explicit acetonitrile at 298 K performed using the GROMACS software package patched with plumed[23] (model description and simulation setup in Supporting Information Section 10).[24] These calculations supported the conclusion that Δ_4-**2** is more favored from an enthalpic point of view, as this difference mainly arises from the difference in potential energy.

Both diastereomers of **2** have flat ligand cores and enclosed cavities, thus rendering **2** a good prospective host for large π-extended guests. We therefore began to investigate the host−guest properties of **2** with fullerenes and fullerene derivatives (Figure 2a). Heating an equimolar mixture of guest and **2** in acetonitrile at 343 K for 30 min resulted in the quantitative formation of the 1:1 host−guest complexes **G⊂2**, as confirmed by ^{1}H NMR, ^{19}F NMR, and ESI-MS spectra for all investigated guests (Supporting Information, Section 6.1). The major contributions to binding were inferred to be extensive stacking interactions between host and guest, as well as solvophobic effects in acetonitrile. The insolubility of these π-extended guests in acetonitrile prevented quantification of binding strength through ^{1}H NMR titration experiments.

^{1}H NMR and CD spectra confirmed that both Δ_4-**2** and Λ_4-**2** were able to accommodate the guests, with **G⊂**Δ_4-**2** as the major species (Figures 2a and S69); $\Delta_4 \rightleftarrows \Lambda_4$ interconversion was also observed during the binding process. We inferred that the size and shape fit between guest and cage change the energy differences between two configurations. To quantify this phenomenon, molecular volume (V_{mol})[21] was used to determine the size of the guest, while sphericity (Ψ)[25] was employed to reflect the shape of the guest considering the near-spherical cavity of **2** (Table S2). The plot of d.r. against V_{mol} and Ψ revealed that binding a smaller and more spherical guest resulted in a stronger energetic preference for the Δ_4 configuration, whereas binding larger and less spherical guests reduced energy differences between diastereomers (Figure 2b). Although the stereochemical effects of guests upon the host observed here were subtle, the model plotted in Figure 2b allowed quantification of guest-induced diastereomer interconversion for binding C_{60} and its adducts, according to the linear relationships between d.r. and V_{mol} and between d.r. and Ψ. However, two outlying points prevented good linear regression fits for binding C_{70} and C_{70}PCBM ([6,6]-phenyl-C_{71}-butyric acid methyl ester).

To obtain information related to the energy barriers for the interconversion between Δ_4-**2** and Λ_4-**2**, we employed multiple infrequent well-tempered metadynamics (WT-MetaD) simulations.[26] These biased simulations allowed us to activate the escape from the two local Δ and Λ minima and to obtain information on the associated barriers and characteristic timescales expected for these transitions in unbiased conditions. In particular, we activated the transition of one of the four metal vertices, exploring the $\Delta_4 \rightarrow \Delta_3\Lambda$ and $\Lambda_4 \rightarrow \Lambda_3\Delta$ transitions (Figure 2c), which are first necessary steps in the $\Delta_4 \rightleftarrows \Lambda_4$ isomerization. Fifty infrequent WT-MetaD simulations were run for both transitions.

For the $\Delta_4 \rightarrow \Delta_3\Lambda$ transition, the infrequent WT-MetaD simulations provided a transition energy barrier $\Delta G^{\ddagger} \sim 24.3$ kcal mol^{-1} and a characteristic transition timescale $\tau \sim 3.2 \times 10^5$ s, while the corresponding energy barrier and timescale for $\Lambda_4 \rightarrow \Lambda_3\Delta$ were calculated to be $\Delta G^{\ddagger} \sim 23.5$ kcal mol^{-1} and $\tau \sim 9.3 \times 10^4$ s, respectively. These results suggested that the dynamics of interconversion between Δ_4 and Λ_4 diastereomers are slow at room temperature. Similar energy barriers were obtained for the diastereomer transformations of $C_{70}\subset$**2**. However, by rescaling the obtained transition timescales at 343 K (mixing condition), we could estimate that these transition events can occur within a timescale of minutes. This suggests that the Δ_4 and Λ_4 configurations dynamically equilibrate during the self-assembly process and reequilibrate during mixing with guest molecules.

We then investigated the ability of **2** to purify high-value fullerenes, starting with preparing a mixture consisting of equimolar amounts of C_{60}, C_{60}PCBM, bis-C_{60}PCBM, and **2** in acetonitrile (Figure 3). Notably, after being kept at 343 K for 30 min, the host−guest complex bis-C_{60}PCBM$\subset$**2** was observed to form exclusively, as confirmed by ESI-MS and ^{1}H NMR (Figures S89 and S90). Likewise, cage **2** was also able to selectively extract C_{70}PCBM from a mixture with C_{70} (Figures S91 and S92). The efficient and selective encapsulation of bis-C_{60}PCBM and C_{70}PCBM by **2** may provide an alternative method for the purification of fullerene covalent adducts contaminated with numerous side-products from reaction mixtures.[27] We attribute the excellent selectivity observed here to the higher solubility of these alkyl chain-substituted fullerenes in organic solvents.[28]

Electron-deficient **2** was also observed to bind electron-rich enantiopure cryptophane-A, which is an example of an important class of organic supramolecular host.[29] The host−guest adduct CRY-A$\subset$**2** was formed upon heating equimolar amounts of CRY-A and **2** in acetonitrile at 343 K for 30 min (Figure 4). *PP*-CRY-A$\subset$**2** (Δ_4:Λ_4 = 2.4:1) retained the stereochemical configuration of the parent cage **2** (Δ_4:Λ_4 = 2.4:1), whereas the encapsulation of *MM*-CRY-A occurred with inversion of host stereochemistry, providing *MM*-CRY-A$\subset$**2** in a d.r. of Δ_4:Λ_4 = 1:2.6. Opposite Cotton effects observed in the CD spectra of both host−guest complexes also confirmed such stereochemical outcomes upon encapsulation of enantiopure CRY-A (Figure S94). The Δ_4 configuration was thus favored by *PP*-CRY-A, whereas the Λ_4 configuration was preferred by *MM*-CRY-A. The inversion of the stereochemistry of **2** induced by *MM*-CRY-A reflected that host **2** can dynamically adapt its stereochemistry and chiral inner void to maximize binding affinity for a chiral guest.

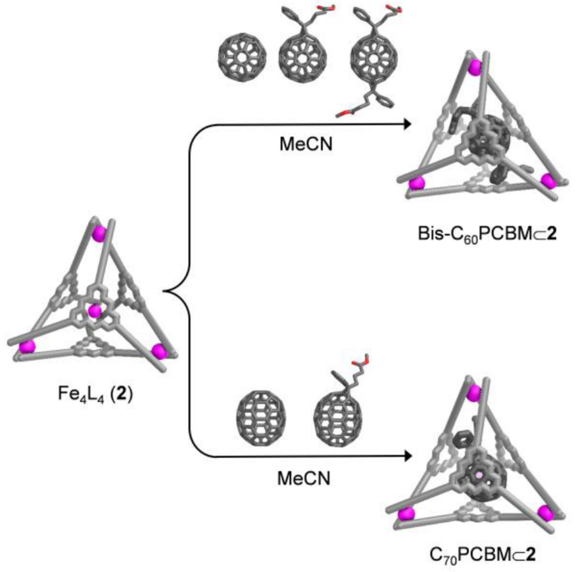

Figure 3. Schematic showing the selective encapsulation of bis-C_{60}PCBM and C_{70}PCBM.

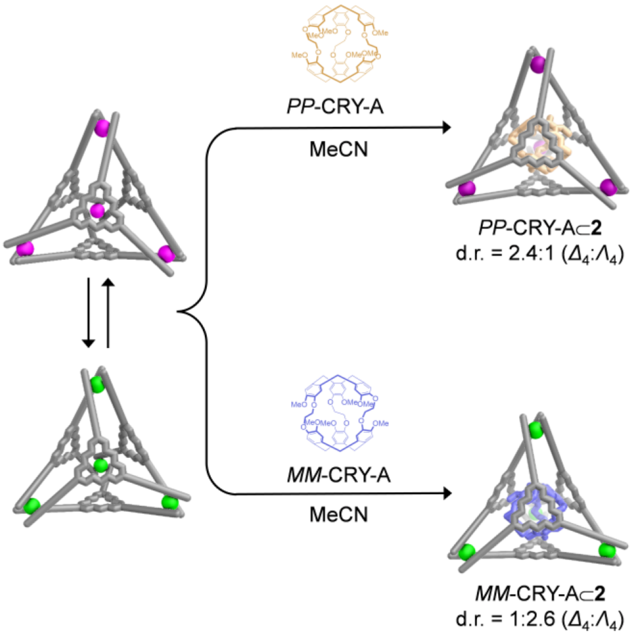

Figure 4. Schematic showing the stereochemical communication between **2** and CRY-A.

We next explored the enantioselective separation of racemic guests by **2**. We observed that **2** displayed no enantioselectivity in binding racemic C_{70}PCBM, as confirmed by ^{1}H NMR and CD spectra (Figures S65 and S105). Diastereoenriched **2** was nonetheless capable of enantioselectively separating racemic CRY-A (Figure 5a).

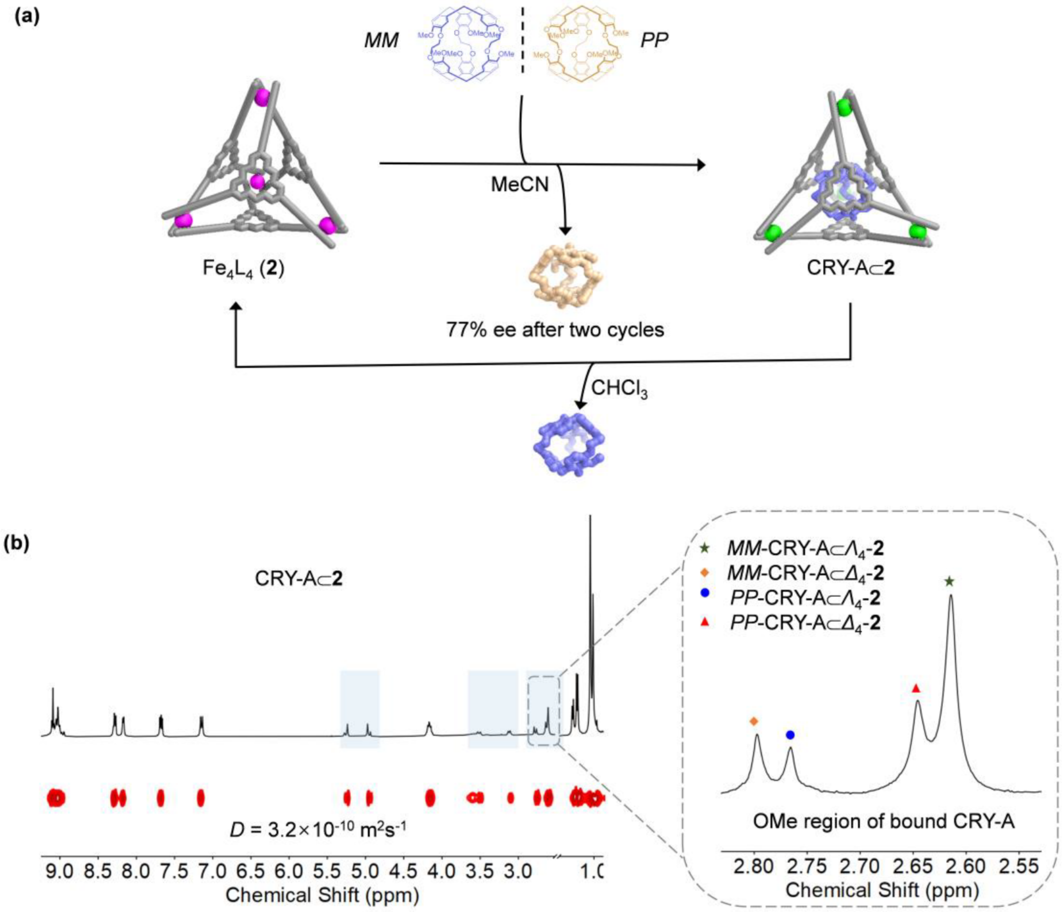

Figure 5. (a) Schematic showing the enantioselective resolution of CRY-A by cage **2** in acetonitrile and the recycling of **2** in chloroform. (b) Partial ^{1}H NMR spectrum of CRY-A$\subset$**2** obtained in the first round of the resolution procedure, with the peaks for the encapsulated guest highlighted with a light blue background, showing an expansion of the OMe region of bound CRY-A (400 MHz, CD_3CN, 298 K).

Two equivalents of racemic CRY-A were added to an acetonitrile solution of **2**, and the reaction mixture was maintained at 343 K for 30 min. The host−guest complex CRY-A$\subset$**2** was isolated by precipitation with diethyl ether; evaporating the excess diethyl ether subsequently afforded unbound CRY-A. All signals in the ^{1}H NMR spectrum of CRY-A$\subset$**2** had the same diffusion coefficient, with proton signals corresponding to bound CRY-A shifted upfield due to host shielding effects (Figure 5b). Four sets of signals from the methoxy groups of CRY-A were observed in the 2.55−2.83 ppm region, indicating that CRY-A$\subset$**2** consists of four diastereomers, *PP*-CRY-A$\subset\Delta_4$-**2**, *PP*-CRY-A$\subset\Lambda_4$-**2**, *MM*-CRY-A$\subset\Delta_4$-**2**, and *MM*-CRY-A$\subset\Lambda_4$-**2**. Comparison with the ^{1}H NMR spectra for *PP*-CRY-A$\subset$**2** and *MM*-CRY-A$\subset$**2** allowed us to identify each diastereomer in solution (Figure S93).

The ^{1}H NMR spectrum clearly showed that more *MM*-CRY-A was encapsulated when two equivalents of racemic guest were used. Cotton effects assigned to *MM*-CRY-A were also observed in the CD spectrum of CRY-A$\subset$**2** (Figure S94). The enantiomeric excess (ee) of the unbound CRY-A was determined to be 32% by chiral HPLC, with *PP*-CRY-A being enriched (Figure S96). The bound CRY-A was released by sonicating a suspension of the host−guest complex in chloroform (Figure S102), and the solid **2** was then recovered by centrifugation (Figures S103 and S104).

In control experiments, *PP*-CRY-A was observed to be encapsulated kinetically faster than *MM*-CRY-A at the initial stage of the binding process, as *PP*-CRY-A is bound more strongly by the Δ_4 configuration of **2** (Δ_4:Λ_4 = 2.4:1 for this guest). Heating the reaction mixture resulted in re-equilibration of the cage framework, eventually giving *MM*-CRY-A$\subset\Lambda_4$-**2** as the major host−guest complex, indicating that *MM*-CRY-A$\subset\Lambda_4$-**2** is the thermodynamically favored diastereomer within the four-diastereomer CRY-A$\subset$**2** system (Figure S101). These results indicated that the enantioselectivity in binding racemic CRY-A by **2** is driven by the formation of the thermodynamically stable host−guest diastereomer, *MM*-CRY-A$\subset\Lambda_4$-**2**.

Encouraged by the chiral resolution observed, we ran a second round of separation experiments, through addition of the CRY-A (32% ee) obtained from the first round to a fresh acetonitrile solution of **2**. After precipitation of the host−guest adduct and removal of the solvent, the unbound CRY-A was obtained in 77% ee, as determined by chiral HPLC (Figure S98).

■ CONCLUSIONS

The moderately stereoselective self-assembly of $Fe^{II}_4L_4$ tetrahedron **2** thus can serve as the basis of an enantioseparation process, based upon a nuanced understanding of how stereochemistry influences guest fit within this host. Cage **2** was also capable of selectively extracting bis-C_{60}PCBM and

C_{70}PCBM from mixtures of their derivatives. The strategy outlined herein may thus become applicable to the design of new cage-based purification methods, particularly stereoselective ones. Future work will focus on the immobilization of such *N*-heterotriangulene-based cages on solid supports, such as alumina, for the development of efficient large-scale separation and purification processes.[30]

■ ASSOCIATED CONTENT

Data Availability Statement

Structure and parameters of the computational models used in atomistic molecular dynamics are available at 10.5281/zenodo.7350671 (ref 24).

Supporting Information

The Supporting Information is available free of charge at https://pubs.acs.org/doi/10.1021/jacs.3c00294.

Experimental procedures; NMR characterizations; mass spectrometry data; CD spectra; volume calculations; HPLC data; computational model parametrization; model simulation protocol (PDF)

■ AUTHOR INFORMATION

Corresponding Authors

Giovanni M. Pavan − *Department of Applied Science and Techology, Politecnico di Torino, 10129 Torino, Italy; Department of Innovative Technologies, University of Applied Sciences and Arts of Southern Switzerland, CH-6962 Lugano-Viganello, Switzerland;* orcid.org/0000-0002-3473-8471; Email: giovanni.pavan@polito.it

Jonathan R. Nitschke − *Yusuf Hamied Department of Chemistry, University of Cambridge, Cambridge CB2 1EW, U.K.;* orcid.org/0000-0002-4060-5122; Email: jrn34@cam.ac.uk

Authors

Weichao Xue − *Yusuf Hamied Department of Chemistry, University of Cambridge, Cambridge CB2 1EW, U.K.;* orcid.org/0000-0002-8376-9485

Luca Pesce − *Department of Innovative Technologies, University of Applied Sciences and Arts of Southern Switzerland, CH-6962 Lugano-Viganello, Switzerland;* orcid.org/0000-0001-6364-9577

Adinarayana Bellamkonda − *Yusuf Hamied Department of Chemistry, University of Cambridge, Cambridge CB2 1EW, U.K.*

Tanya K. Ronson − *Yusuf Hamied Department of Chemistry, University of Cambridge, Cambridge CB2 1EW, U.K.;* orcid.org/0000-0002-6917-3685

Kai Wu − *Yusuf Hamied Department of Chemistry, University of Cambridge, Cambridge CB2 1EW, U.K.;* orcid.org/0000-0001-6336-7836

Dawei Zhang − *Shanghai Key Laboratory of Green Chemistry and Chemical Processes, School of Chemistry and Molecular Engineering, East China Normal University, Shanghai 200062, China;* orcid.org/0000-0002-0898-9795

Nicolas Vanthuyne − *Aix Marseille Université, Centrale Marseille, CNRS, iSm2 UMR 7313, 13397 Marseille, France;* orcid.org/0000-0003-2598-7940

Thierry Brotin − *Laboratoire de Chimie, Université Lyon, Ens de Lyon, Lyon F69342, France;* orcid.org/0000-0001-9746-4706

Alexandre Martinez − *Aix Marseille Université, Centrale Marseille, CNRS, iSm2 UMR 7313, 13397 Marseille, France;* orcid.org/0000-0002-6745-5734

Complete contact information is available at: https://pubs.acs.org/10.1021/jacs.3c00294

Notes

The authors declare no competing financial interest.

■ ACKNOWLEDGMENTS

This study was supported by the European Research Council (695009) and the UK Engineering and Physical Sciences Research Council (EPSRC, EP/T031603/1 and EP/P027067/1). W.X. thanks the Deutsche Forschungsgemeinschaft (DFG) for a postdoctoral fellowship. G.M.P. acknowledges funding received from the Swiss National Science Foundation (IZLIZ2_183336) and the European Research Council (818776). G.M.P. and L.P. also acknowledge the computational resources provided by the Swiss National Supercomputing Center (CSCS). We acknowledge the Department of Chemistry NMR facility, University of Cambridge, for performing some NMR experiments.

■ REFERENCES

(1) Koshland, D. E., Jr. The Key−Lock Theory and the Induced Fit Theory. *Angew. Chem., Int. Ed.* **1995**, *33*, 2375−2378.

(2) Bell, E. L.; Finnigan, W.; France, S. P.; Green, A. P.; Hayes, M. A.; Hepworth, L. J.; Lovelock, S. L.; Niikura, H.; Osuna, S.; Romero, E.; Ryan, K. S.; Turner, N. J.; Flitsch, S. L. Biocatalysis. *Nat. Rev. Methods Primers* **2021**, *1*, 46.

(3) Mislow, K.; Siegel, J. Stereoisomerism and Local Chirality. *J. Am. Chem. Soc.* **1984**, *106*, 3319−3328.

(4) For comprehensive reviews on metal−organic cages, see: (a) Seeber, G.; Tiedemann, B. E. F.; Raymond, K. N. Supramolecular Chirality in Coordination Chemistry. *Top Curr. Chem.* **2006**, *265*, 147−183. (b) Chen, L.-J.; Yang, H.-B.; Shionoya, M. Chiral Metallosupramolecular Architectures. *Chem. Soc. Rev.* **2017**, *46*, 2555−2576. (c) Pan, M.; Wu, K.; Zhang, J.-H.; Su, C.-Y. Chiral Metal−Organic Cages/Containers (MOCs): From Structural and Stereochemical Design to Applications. *Coord. Chem. Rev.* **2019**, *378*, 333−349. (d) Gosselin, A. J.; Rowland, C. A.; Bloch, E. D. Permanently Microporous Metal−Organic Polyhedra. *Chem. Rev.* **2020**, *120*, 8987−9014.

(5) For selected examples on chiral sensing, recognition, and separation by cages, see: (a) Fiedler, D.; Leung, D. H.; Bergman, R. G.; Raymond, K. N. Enantioselective Guest Binding and Dynamic Resolution of Cationic Ruthenium Complexes by a Chiral Metal−Ligand Assembly. *J. Am. Chem. Soc.* **2004**, *126*, 3674−3675. (b) Liu, T.; Liu, Y.; Xuan, W.; Cui, Y. Chiral Nanoscale Metal-Organic Tetrahedral Cages: Diastereoselective Self-Assembly and Enantioselective Separation. *Angew. Chem., Int. Ed.* **2010**, *49*, 4121−4124. (c) Xuan, W.; Zhang, M.; Liu, Y.; Chen, Z.; Cui, Y. A Chiral Quadruple-Stranded Helicate Cage for Enantioselective Recognition and Separation. *J. Am. Chem. Soc.* **2012**, *134*, 6904−6907. (d) Dong, J.; Zhou, Y.; Zhang, F.; Cui, Y. A Highly Fluorescent Metallosalalen-Based Chiral Cage for Enantioselective Recognition and Sensing. *Chem.—Eur. J.* **2014**, *20*, 6455−6461. (e) Bolliger, J. L.; Belenguer, A. M.; Nitschke, J. R. Enantiopure Water-Soluble [Fe_4L_6] Cages: Host−Guest Chemistry and Catalytic Activity. *Angew. Chem., Int. Ed.* **2013**, *52*, 7958−7962. (f) Wu, K.; Li, K.; Hou, Y.-J.; Pan, M.; Zhang, L.-Y.; Chen, L.; Su, C.-Y. Homochiral D_4-Symmetric Metal−Organic Cages from Stereogenic Ru(II) Metalloligands for Effective Enantioseparation of Atropisomeric Molecules. *Nat. Commun.* **2016**, *7*, 10487. (g) Schulte, T. R.; Holstein, J. J.; Clever, G. H. Chiral Self-Discrimination and Guest Recognition in Helicene-Based Coordination Cages. *Angew. Chem., Int. Ed.* **2019**, *58*, 5562−5566.

(h) Howlader, P.; Zangrando, E.; Mukherjee, P. S. Self-Assembly of Enantiopure Pd_{12} Tetrahedral Homochiral Nanocages with Tetrazole Linkers and Chiral Recognition. *J. Am. Chem. Soc.* **2020**, *142*, 9070−9078. (i) Yang, Y.; Ronson, T. K.; Lu, Z.; Zheng, J.; Vanthuyne, N.; Martinez, A.; Nitschke, J. R. A Curved Host and Second Guest Cooperatively Inhibit the Dynamic Motion of Corannulene. *Nat. Commun.* **2021**, *12*, 4079. (j) Zhu, C.; Tang, H.; Yang, K.; Fang, Y.; Wang, K.-Y.; Xiao, Z.; Wu, X.; Li, Y.; Powell, J. A.; Zhou, H.-C. Homochiral Dodecanuclear Lanthanide "Cage in Cage" for Enantioselective Separation. *J. Am. Chem. Soc.* **2021**, *143*, 12560−12566.

(6) For reviews on cage catalysis, see: (a) Brown, C. J.; Toste, F. D.; Bergman, R. G.; Raymond, K. N. Supramolecular Catalysis in Metal−Ligand Cluster Hosts. *Chem. Rev.* **2015**, *115*, 3012−3035. (b) Tan, C.; Chu, D.; Tang, X.; Liu, Y.; Xuan, W.; Cui, Y. Supramolecular Coordination Cages for Asymmetric Catalysis. *Chem.—Eur. J.* **2019**, *25*, 662−672. (c) Wang, K.; Jordan, J. H.; Hu, X.-Y.; Wang, L. Supramolecular Strategies for Controlling Reactivity within Confined Nanospaces. *Angew. Chem., Int. Ed.* **2020**, *59*, 13712−13721. (d) Morimoto, M.; Bierschenk, S. M.; Xia, K. T.; Bergman, R. G.; Raymond, K. N.; Toste, F. D. Advances in Supramolecular Host-Mediated Reactivity. *Nat. Catal.* **2020**, *3*, 969−984. (e) Olivo, G.; Capocasa, G.; Del Giudice, D.; Lanzalunga, O.; Di Stefano, S. New Horizons for Catalysis Disclosed by Supramolecular Chemistry. *Chem. Soc. Rev.* **2021**, *50*, 7681−7724.

(7) For selected examples on enantioselective cage catalysis, see: (a) Nishioka, Y.; Yamaguchi, T.; Kawano, M.; Fujita, M. Asymmetric [2 + 2] Olefin Cross Photoaddition in a Self-Assembled Host with Remote Chiral Auxiliaries. *J. Am. Chem. Soc.* **2008**, *130*, 8160−8161. (b) Brown, C. J.; Bergman, R. G.; Raymond, K. N. Enantioselective Catalysis of the Aza-Cope Rearrangement by a Chiral Supramolecular Assembly. *J. Am. Chem. Soc.* **2009**, *131*, 17530−17531. (c) Gadzikwa, T.; Bellini, R.; Dekker, H. L.; Reek, J. N. H. Self-Assembly of a Confined Rhodium Catalyst for Asymmetric Hydroformylation of Unfunctionalized Internal Alkenes. *J. Am. Chem. Soc.* **2012**, *134*, 2860−2863. (d) Wang, Z. J.; Clary, K. N.; Bergman, R. G.; Raymond, K. N.; Toste, F. D. A Supramolecular Approach to Combining Enzymatic and Transition Metal Catalysis. *Nat. Chem.* **2013**, *5*, 100−103. (e) Zhao, C.; Sun, Q.-F.; Hart-Cooper, W. M.; DiPasquale, A. G.; Toste, F. D.; Bergman, R. G.; Raymond, K. N. Chiral Amide Directed Assembly of a Diastereo- and Enantiopure Supramolecular Host and its Application to Enantioselective Catalysis of Neutral Substrates. *J. Am. Chem. Soc.* **2013**, *135*, 18802−18805. (f) García-Simón, C.; Gramage-Doria, R.; Raoufmoghaddam, S.; Parella, T.; Costas, M.; Ribas, X.; Reek, J. N. H. Enantioselective Hydroformylation by a Rh-Catalyst Entrapped in a Supramolecular Metallocage. *J. Am. Chem. Soc.* **2015**, *137*, 2680−2687. (g) Ueda, Y.; Ito, H.; Fujita, D.; Fujita, M. Permeable Self-Assembled Molecular Containers for Catalyst Isolation Enabling Two-Step Cascade Reactions. *J. Am. Chem. Soc.* **2017**, *139*, 6090−6093. (h) Guo, J.; Xu, Y.-W.; Li, K.; Xiao, L.-M.; Chen, S.; Wu, K.; Chen, X.-D.; Fan, Y.-Z.; Liu, J.-M.; Su, C.-Y. Regio- and Enantioselective Photodimerization within the Confined Space of a Homochiral Ruthenium/Palladium Heterometallic Coordination Cage. *Angew. Chem., Int. Ed.* **2017**, *56*, 3852−3856. (i) Tan, C.; Jiao, J.; Li, Z.; Liu, Y.; Han, X.; Cui, Y. Design and Assembly of a Chiral Metallosalen-Based Octahedral Coordination Cage for Supramolecular Asymmetric Catalysis. *Angew. Chem., Int. Ed.* **2018**, *57*, 2085−2090. (j) Jiao, J.; Tan, C.; Li, Z.; Liu, Y.; Han, X.; Cui, Y. Design and Assembly of Chiral Coordination Cages for Asymmetric Sequential Reactions. *J. Am. Chem. Soc.* **2018**, *140*, 2251−2259. (k) Guo, J.; Fan, Y.-Z.; Lu, Y.-L.; Zheng, S.-P.; Su, C.-Y. Visible-Light Photocatalysis of Asymmetric [2 + 2] Cycloaddition in Cage-Confined Nanospace Merging Chirality with Triplet-State Photosensitization. *Angew. Chem., Int. Ed.* **2020**, *59*, 8661−8669.

(8) (a) Zhou, J.; Rao, L.; Yu, G.; Cook, T. R.; Chen, X.; Huang, F. Supramolecular Cancer Nanotheranostics. *Chem. Soc. Rev.* **2021**, *50*, 2839−2891. (b) Zhu, H.; Li, Q.; Zhu, W.; Huang, F. Pillararenes as Versatile Building Blocks for Fluorescent Materials. *Acc. Mater. Res.* **2022**, *3*, 658−668.

(9) (a) Terpin, A. J.; Ziegler, M.; Johnson, D. W.; Raymond, K. N. Resolution and Kinetic Stability of a Chiral Supramolecular Assembly Made of Labile Components. *Angew. Chem., Int. Ed.* **2001**, *40*, 157−160. (b) Ikeda, A.; Udzu, H.; Zhong, Z.; Shinkai, S.; Sakamoto, S.; Yamaguchi, K. A Self-Assembled Homooxacalix[3]arene-based Dimeric Capsule Constructed by a Pd^{II}−Pyridine Interaction Which Shows a Novel Chiral Twisting Motion in Response to Guest Inclusion. *J. Am. Chem. Soc.* **2001**, *123*, 3872−3877. (c) Davis, A. V.; Fiedler, D.; Ziegler, M.; Terpin, A.; Raymond, K. N. Resolution of Chiral, Tetrahedral M_4L_6 Metal−Ligand Hosts. *J. Am. Chem. Soc.* **2007**, *129*, 15354−15363. (d) Wan, S.; Lin, L.-R.; Zeng, L.; Lin, Y.; Zhang, H. Efficient Optical Resolution of Water-Soluble Self-Assembled Tetrahedral M_4L_6 Cages with 1,1′-Bi-2-naphthol. *Chem. Commun.* **2014**, *50*, 15301−15304. (e) Bonakdarzadeh, P.; Pan, F.; Kalenius, E.; Jurček, O.; Rissanen, K. Spontaneous Resolution of an Electron-Deficient Tetrahedral Fe_4L_4 Cage. *Angew. Chem., Int. Ed.* **2015**, *54*, 14890−14893. (f) Luo, D.; Wang, X.-Z.; Yang, C.; Zhou, X.-P.; Li, D. Self-Assembly of Chiral Metal−Organic Tetartoid. *J. Am. Chem. Soc.* **2018**, *140*, 118−121. (g) Hou, Y.-J.; Wu, K.; Wei, Z.-W.; Li, K.; Lu, Y.-L.; Zhu, C.-Y.; Wang, J.-S.; Pan, M.; Jiang, J.-J.; Li, G.-Q.; Su, C.-Y. Design and Enantioresolution of Homochiral Fe(II)−Pd(II) Coordination Cages from Stereolabile Metalloligands: Stereochemical Stability and Enantioselective Separation. *J. Am. Chem. Soc.* **2018**, *140*, 18183−18191. (h) Zhang, D.; Ronson, T. K.; Greenfield, J. L.; Brotin, T.; Berthault, P.; Léonce, E.; Zhu, J.-L.; Xu, L.; Nitschke, J. R. Enantiopure $[Cs^+/Xe\subset Cryptophane]\subset Fe^{II}{}_4L_4$ Hierarchical Superstructures. *J. Am. Chem. Soc.* **2019**, *141*, 8339−8345. (i) Howlader, P.; Mondal, S.; Ahmed, S.; Mukherjee, P. S. Guest-Induced Enantioselective Self-Assembly of a Pd_6 Homochiral Octahedral Cage with a C_3-Symmetric Pyridyl Donor. *J. Am. Chem. Soc.* **2020**, *142*, 20968−20972.

(10) (a) Chepelin, O.; Ujma, J.; Wu, X.; Slawin, A. M. Z.; Pitak, M. B.; Coles, S. J.; Michel, J.; Jones, A. C.; Barran, P. E.; Lusby, P. J. Luminescent, Enantiopure, Phenylatopyridine Iridium-Based Coordination Capsules. *J. Am. Chem. Soc.* **2012**, *134*, 19334−19337. (b) Ren, D.-H.; Qiu, D.; Pang, C.-Y.; Li, Z.; Gu, Z.-G. Chiral Tetrahedral Iron (II) Cages: Diastereoselective Subcomponent Self-Assembly, Structure Interconversion and Spin-Crossover Properties. *Chem. Commun.* **2015**, *51*, 788−791. (c) Yang, Y.; Jia, J.-H.; Pei, X.-L.; Zheng, H.; Nan, Z.-A.; Wang, Q.-M. Diastereoselective Synthesis of *O* Symmetric Heterometallic Cubic Cages. *Chem. Commun.* **2015**, *51*, 3804−3807. (d) Martir, D. R.; Escudero, D.; Jacquemin, D.; Cordes, D. B.; Slawin, A. M. Z.; Fruchtl, H. A.; Warriner, S. L.; Zysman-Colman, E. Homochiral Emissive Λ_8- and Δ_8-$[Ir_8Pd_4]^{16+}$ Supramolecular Cages. *Chem.—Eur. J.* **2017**, *23*, 14358−14366. (e) Sun, B.; Nurttila, S. S.; Reek, J. N. H. Synthesis and Characterization of Self-Assembled Chiral $Fe^{II}{}_2L_3$ Cages. *Chem.—Eur. J.* **2018**, *24*, 14693−14700. (f) Zhu, H.; Li, Q.; Shi, B.; Xing, H.; Sun, Y.; Lu, S.; Shangguan, L.; Li, X.; Huang, F.; Stang, P. J. Formation of Planar Chiral Platinum Triangles via Pillar[5]arene for Circularly Polarized Luminescence. *J. Am. Chem. Soc.* **2020**, *142*, 17340−17345. (g) Jiao, J.; Dong, J.; Li, Y.; Cui, Y. Fine-Tuning of Chiral Microenvironments within Triple-Stranded Helicates for Enhanced Enantioselectivity. *Angew. Chem., Int. Ed.* **2021**, *60*, 16568−16575.

(11) (a) Castilla, A. M.; Ramsay, W. J.; Nitschke, J. R. Stereochemistry in Subcomponent Self-Assembly. *Acc. Chem. Res.* **2014**, *47*, 2063−2073. (b) Martir, D. R.; Zysman-Colman, E. Photoactive Supramolecular Cages Incorporating Ru(II) and Ir(III) Metal Complexes. *Chem. Commun.* **2019**, *55*, 139−158.

(12) (a) Yan, L.-L.; Tan, C.-H.; Zhang, G.-L.; Zhou, L.-P.; Bünzli, J.-C.; Sun, Q.-F. Stereocontrolled Self-Assembly and Self-Sorting of Luminescent Europium Tetrahedral Cages. *J. Am. Chem. Soc.* **2015**, *137*, 8550−8555. (b) Yeung, C.-T.; Yim, K.-H.; Wong, H.-Y.; Pal, R.; Lo, W.-S.; Yan, S.-C.; Yee-Man Wong, M.; Yufit, D.; Smiles, D. E.; McCormick, L. J.; Teat, S. J.; Shuh, D. K.; Wong, W.-T.; Law, G.-L. Chiral Transcription in Self-Assembled Tetrahedral Eu_4L_6 Chiral Cages Displaying Sizable Circularly Polarized Luminescence. *Nat.*

Commun. **2017**, *8*, 1128. (c) Zhou, Y.; Li, H.; Zhu, T.; Gao, T.; Yan, P. A Highly Luminescent Chiral Tetrahedral $Eu_4L_4(L')_4$ Cage: Chirality Induction, Chirality Memory, and Circularly Polarized Luminescence. *J. Am. Chem. Soc.* **2019**, *141*, 19634−19643. (d) Hu, S.-J.; Guo, X.-Q.; Zhou, L.-P.; Yan, D.-N.; Cheng, P.-M.; Cai, L.-X.; Li, X.-Z.; Sun, Q.-F. Guest-Driven Self-Assembly and Chiral Induction of Photofunctional Lanthanide Tetrahedral Cages. *J. Am. Chem. Soc.* **2022**, *144*, 4244−4253.

(13) Takezawa, H.; Murase, T.; Resnati, G.; Metrangolo, P.; Fujita, M. Recognition of Polyfluorinated Compounds Through Self-Aggregation in a Cavity. *J. Am. Chem. Soc.* **2014**, *136*, 1786−1788.

(14) Xue, W.; Ronson, T. K.; Lu, Z.; Nitschke, J. R. Solvent Drives Switching between Λ and Δ Metal Center Stereochemistry of M_8L_6 Cubic Cages. *J. Am. Chem. Soc.* **2022**, *144*, 6136−6142.

(15) (a) Crowley, J. D.; Lisboa, L. S.; van Hilst, Q. V. C. Supramolecular Systems: Metallo-Molecular Machines and Stimuli Responsive Metallo-Macrocycles and Cages. In *Comprehensive Coordination Chemistry III*,; Constable, E. C.; Parkin, G.; Que, L., Jr., Eds.; Elsevier: Oxford, 2021; pp 174−205. (b) Hauke, C. E.; Cook, T. R. Self-Assembly Processes for the Construction of Supramolecular Coordination Compounds. In *Comprehensive Coordination Chemistry III*; Constable, E. C.; Parkin, G.; Que, L., Jr., Eds.; Elsevier: Oxford, 2021; pp 1074−1085. (c) Lewis, J. E. M. Molecular Engineering of Confined Space in Metal−Organic Cages. *Chem. Commun.* **2022**, *58*, 13873−13886.

(16) Symmers, P. R.; Burke, M. J.; August, D. P.; Thomson, P. I. T.; Nichol, G. S.; Warren, M. R.; Campbell, C. J.; Lusby, P. J. Non-Equilibrium Cobalt(III) "Click" Capsules. *Chem. Sci.* **2015**, *6*, 756−760.

(17) McConnell, A. J.; Aitchison, C. M.; Grommet, A. B.; Nitschke, J. R. Subcomponent Exchange Transforms an $Fe^{II}{}_4L_4$ Cage from High- to Low-Spin, Switching Guest Release in a Two-Cage System. *J. Am. Chem. Soc.* **2017**, *139*, 6294−6297.

(18) Ziegler, M.; von Zelewsky, A. Charge-Transfer Excited State Properties of Chiral Transition Metal Coordination Compounds Studied by Chiroptical Spectroscopy. *Coord. Chem. Rev.* **1998**, *177*, 257−300.

(19) (a) Hidaka, J.; Douglas, B. E. Circular Dichroism of Coordination Compounds. II. Some Metal Complexes of 2,2′-Dipyridyl and 1,10-Phenanthroline. *Inorg. Chem.* **1964**, *3*, 1180−1184. (b) Mason, S. F.; Peart, B. J. Optical Rotatory Power of Coordination Compounds. Part XVII. The Circular Dichroism of Trisbipyridyl and Trisphenanthroline Complexes. *J. Chem. Soc., Dalton Trans.* **1973**, 949−955.

(20) (a) Becke, A. D. Density-Functional Thermochemistry. III. The Role of Exact Exchange. *J. Chem. Phys.* **1993**, *98*, 5648−5652. (b) *Gaussian 16, Revision C.01*; Gaussian, Inc.: Wallingford, CT, 2016, https://gaussian.com/gaussian16.

(21) The the internal cavity volumes of Δ_4-**2** and Λ_4-**2** and volumes of guests were calculated using the MoloVol program; see: Maglic, J. B.; Lavendomme, R. MoloVol: An Easy-to-Use Program for Analyzing Cavities, Volumes and Surface Areas of Chemical Structures. *J. Appl. Crystallogr.* **2022**, *55*, 1033−1044.

(22) (a) Ousaka, N.; Clegg, J. K.; Nitschke, J. R. Nonlinear Enhancement of Chiroptical Response through Subcomponent Substitution in M_4L_6 Cages. *Angew. Chem., Int. Ed.* **2012**, *51*, 1464−1468. (b) Castilla, A. M.; Miller, M. A.; Nitschke, J. R.; Smulders, M. M. J. Quantification of Stereochemical Communication in Metal−Organic Assemblies. *Angew. Chem., Int. Ed.* **2016**, *55*, 10616−10620.

(23) (a) Hess, B.; Kutzner, C.; van der Spoel, D.; Lindahl, E. GROMACS 4: Algorithms for Highly Efficient, Load-Balanced, and Scalable Molecular Simulation. *J. Chem. Theory Comput.* **2008**, *4*, 435−447. (b) *GROMACS Release 2020.2*; GROMACS development team: Uppsala, Sweden, 2020, https://manual.gromacs.org/2020.2. (c) Tribello, G. A.; Bonomi, M.; Branduardi, D.; Camilloni, C.; Bussi, G. PLUMED 2: New Feathers for an Old Bird. *Comput. Phys. Commun.* **2014**, *185*, 604−613.

(24) Pesce, L.; Pavan, G. M.Computational data supporting: "Subtle Stereochemical Effects Influence Binding and Purification Abilities of an $Fe^{II}{}_4L_4$ Cage", v1.0; *Zenodo* 2021, https://zenodo.org/record/7350671.

(25) Sabirov, D. S.; Garipova, R. R. The Increase in the Fullerene Cage Volume upon its Chemical Functionalization. *Fuller. Nanotub. Carbon Nanostructures* **2019**, *27*, 702−709.

(26) (a) Tiwary, P.; Parrinello, M. From Metadynamics to Dynamics. *Phys. Rev. Lett.* **2013**, *111*, 230602. (b) Salvalaglio, M.; Tiwary, P.; Parrinello, M. Assessing the Reliability of the Dynamics Reconstructed from Metadynamics. *J. Chem. Theory Comput.* **2014**, *10*, 1420−1425. (c) Barducci, A.; Bussi, G.; Parrinello, M. Well-Tempered Metadynamics: A Smoothly Converging and Tunable Free-Energy Method. *Phys. Rev. Lett.* **2008**, *100*, 020603. (d) Pesce, L.; Perego, C.; Grommet, A. B.; Klajn, R.; Pavan, G. M. Molecular Factors Controlling the Isomerization of Azobenzenes in the Cavity of a Flexible Coordination Cage. *J. Am. Chem. Soc.* **2020**, *142*, 9792−9802.

(27) (a) García-Simón, C.; Costas, M.; Ribas, X. Metallosupramolecular Receptors for Fullerene Binding and Release. *Chem. Soc. Rev.* **2016**, *45*, 40−62. (b) Fuertes-Espinosa, C.; Pujals, M.; Ribas, X. Supramolecular Purification and Regioselective Functionalization of Fullerenes and Endohedral Metallofullerenes. *Chem.* **2020**, *6*, 3219−3262.

(28) Wang, C. I.; Hua, C. C. Solubility of C_{60} and PCBM in Organic Solvents. *J. Phys. Chem. B* **2015**, *119*, 14496−14504.

(29) (a) Brotin, T.; Vanthuyne, N.; Cavagnat, D.; Ducasse, L.; Buffeteau, T. Chiroptical Properties of Nona- and Dodecamethoxy Cryptophanes. *J. Org. Chem.* **2014**, *79*, 6028−6036. (b) Zhang, D.; Martinez, A.; Dutasta, J.-P. Emergence of Hemicryptophanes: From Synthesis to Applications for Recognition, Molecular Machines, and Supramolecular Catalysis. *Chem. Rev.* **2017**, *117*, 4900−4942.

(30) Ryan, H. P.; Haynes, C. J. E.; Smith, A.; Grommet, A. B.; Nitschke, J. R. Guest Encapsulation within Surface-Adsorbed Self-Assembled Cages. *Adv. Mater.* **2021**, *33*, 2004192.